Energy Relaxation Dynamics and Universal Scaling Laws in Organic Light-Emitting Diodes

ERIC R. BITTNER, STOYAN KARABUNARLIEV

Department of Chemistry, University of Houston, Houston, TX 77204-5003

Received 25 February 2003; accepted 10 June 2003

DOI 10.1002/qua.10754

ABSTRACT: Electron–hole (e–h) capture in luminescent conjugated polymers (LCPs) is modeled by the dissipative dynamics of a multilevel electronic system coupled to a phonon bath. Electroinjected e–h pairs are simulated by a mixed quantum state, which relaxes via phonon-driven internal conversions to low-lying charge-transfer (CT) and excitonic (XT) states. The underlying two-band polymer model reflects PPV and spans monoexcited configuration interaction singlets (S) and triplets (T), coupled to Franck–Condon active C═C stretches and ring torsions. Focusing entirely upon long PPV chains, we consider the recombination kinetics of an initially separated CT pair. Our model calculations indicate that S and T recombination proceeds according to a branched, two-step mechanism dictated by near e–h symmetry. The initial relaxation occurs rapidly with nearly half of the population going into excitons (S_{XT} or T_{XT}), while the remaining portion remains locked in metastable CT states. While formation rates of S_{CT} and T_{CT} are nearly equal, S_{XT} is formed about twice as fast T_{XT} in concurrence with experimental observations of these systems. Further, breaking e–h symmetry suppresses the XT to CT branching ratio for triplets and opens a slow CT → XT conversion channel exclusively for singlets due to dipole–dipole interactions between geminate and nongeminate configurations. Finally, our calculations yield a remarkable linear relation between chain length and singlet/triplet branching ratio that can be explained in terms of the binding energies of the respective final excitonic states and the scaling of singlet–triplet energy gap with chain length. Int J Quantum Chem 95: 521–531, 2003

Key words: conjugated polymers; electronic relaxation; Wannier functions; electron/hole symmetry

Introduction

Since the discovery of electroluminescence (EL) in poly(p-phenylene vinylene) PPV [1] considerable efforts have gone into the development and commercialization of light-emitting diodes (LEDs), based on luminescent conjugated polymers (LCPs). While much progress has been made in improving emission efficiency and color control [2], the detailed physics of charge transport and light generation in these materials is relatively poorly understood in comparison with inorganic semiconductors. The 1-D delocalization of electrons and

Correspondence to: E. R. Bittner; email: bittner@uh.edu

substantial electron–hole (e–h) and electron–lattice interactions render the delineation of neutral and charged excitations in LCPs very complex and demanding. Moreover, a dynamic description is needed to capture the transient relaxation processes that occur when charged species approach each other, recombine, and decay.

Photogenerated singlet e–h pairs in LCPs typically relax to highly emissive S_1 excitons prior to decay. In contrast, electroinjected electrons (e^-) and holes (h^+) are not spin correlated and can combine to form both singlet and triplet excitons.

$$e^- + h^+ \begin{array}{l} \xrightarrow{k_S} S_1 \xrightarrow{k_{\mathrm{rad}}} S_o + h\nu \\ \xrightarrow{k_T} T_1 \xrightarrow{k_{so}} S_o. \end{array} \tag{1}$$

Because the decay of the triplet exciton T_1 is nearly radiationless and relaxation to S_o occurs via spin–orbit coupling, quantum efficiency in electroluminescence (η_{EL}) is only a fraction of that for photoluminescence (η_{PL}). If the rate of e–h capture is spin independent, S_1 and T_1 excitons are formed in a 1:3 ratio as dictated by spin degeneracy. In such a case, 75% of the bound e–h pairs are nonemissive, leading to a theoretical maximum of $\eta_{\mathrm{EL}} = 0.25\eta_{\mathrm{PL}}$. Nonetheless, efficiencies of up to $\eta_{\mathrm{EL}} = 0.50\eta_{\mathrm{PL}}$ have been achieved independently on PPV-based LEDs in the laboratories of Heeger [3] and Friend [2]. From this it has been inferred that in organic light-emitting polymers singlet e–h capture is intrinsically more efficient than the respective triplet process ($k_S > k_T$).

If we assume that the formation kinetics is first order such that the singlet and triplet exciton population formation rates are proportional to the total population of charge-transfer (CT) states in the system, then the formation cross-section σ_S for singlet excitons as given by the ratio of singlets to total excitons by

$$\sigma_S = \frac{N_S(t)}{N_S(t) + 3N_T(t)} = \frac{r}{r+3}, \tag{2}$$

where $r = k_S/k_T = \sigma_S/\sigma_T$. To obtain the nearly 64% EL efficiencies reported by various groups [2, 3] in various organic polymer LED devices, r must be in the range of $3 < r < 5$. Such ratios were also obtained for a wide range of organic LCPs via photoabsorption/detection of magnetic resonance (PADMR) experiments by Wohlgenannt et al. [4, 5], which measures the population of photogenerated intrachain parallel and antiparallel polaron pairs in the presence of a magnetic field. This later work [5] is in particular significant in that it establishes a universal linear scaling relationship between r and inverse conjugation length, which holds for a wide range of LCP systems.

Various mechanisms favoring the formation of S_1 vs. T_1 have been proposed for both inter- and intrachain e–h collisions. Using Fermi's golden rule, Shuai et al. [6, 7] indicate that the S cross-section for interchain recombination can be higher than the triplet one due to bond–charge correlations. Wohlgenannt et al. [4] resorted to a similar model of two parallel polyene chains. Both of these works neglect vibronic and relaxation effects. In simulating the intrachain collision of opposite polarons, Kobrak and Bittner [8, 9] showed that formation of S_1 is enhanced by the near-resonance with the free e–h pair. The result reflects the fact that spin-exchange renders T_1 more tightly bound than S_1 [10, 11] and hence more electronic energy must be dissipated by the phonons in the formation of the former. The energy conservation constraints in spin-dependent e–h recombination have been analyzed by Burin and Ratner [12] in an essential-state model. The authors point out that nonradiative processes (internal conversion, intersystem crossing) must entail C═C stretching vibrons because these modes couple most strongly to $\pi \rightarrow \pi^*$ excitations. Recent work by Tandon et al. suggest that irrespective of the recombination process, interchain or intrachain, the *direct transition* to form singlets should always be easier than triplets due to its smaller binding energy relative to the triplet [13]. Last, a comprehensive review of detailing the experiments and theory of this effect was recently presented by Wohlgenannt and Vardeny [14].

In this work, we describe e–h capture in LCPs in terms of the dissipative dynamics of a multilevel electronic system coupled to a phonon bath. Our model is based upon a two-band polymer model introduced by Soos et al. [15, 16] augmented by the coupling of electronic excitations to a bath of vibrational modes. First, we review a time-dependent model for simulating via quantum chemical methods the transient relaxation dynamics of an excited state in an extended system [17, 18]. The methodology we develop herein is applicable to both excitonic transfer (i.e., Förster) as well as charge-transfer states in a general conjugated polymer system. At present, we restrict our attention to monoexcited closed-shell systems; however, the approach can be

extended to the general case for radicals. Second, we examine a specific physical process involving the collision and relaxation of injected e–h pairs in luminescent conjugated polymers, such as PPV [19]. Our calculations underscore the role that vibronic coupling and e–h symmetry play in determining the singlet–triplet branching ratio as the CT state relaxes to form bound e–h excitonic pairs. Finally, we explore the relation between chain length and the singlet/triple branching ratio. We show that our methodology reproduces the remarkably universal linear relation between conjugation length and r as evident in a wide range of conjugated polymer materials. Our model accurately reproduces this linear relation for a specific molecular system and provides a rationalization based upon the variation of the exchange energy with increasing chain length.

Methodology

TWO-BAND POLYMER MODEL + PHONONS

The Hamiltonian for the coupled system is

$$H = H_{\mathrm{el}} + H_{\mathrm{ph}} + H_{\mathrm{el-ph}} = \sum_{mn} (F^o_{mn} + V_{mn})|\mathbf{m}\rangle\langle\mathbf{n}| + \frac{1}{2}\sum_{\mu\nu} (\kappa_{\mu-\nu} q_\mu q_\nu + \delta_{\mu\nu} p_\mu^2) + \sum_{mn\mu} \left(\frac{\partial F_{mn}}{\partial q_\mu}\right)_o q_\mu |\mathbf{m}\rangle\langle\mathbf{n}|. \quad (3)$$

The electronic Hamiltonian H_{el} represents the configuration interaction of localized singlet or triplet configurations $|\mathbf{m}\rangle = |\bar{m}n\rangle$ with a valance hole in repeat unit $\bar{m}$ and a conduction electron in repeat unit n. For example, the $|\bar{3}3\rangle$ geminate monoexcited configuration for a 6 repeat-unit system is

$$|\bar{m}m\rangle = (\odot - \odot - \otimes - \odot - \odot - \odot), \quad (4)$$

whereas

$$|\bar{m}n\rangle = (\odot - \oplus - \odot - \odot - \ominus - \odot) \quad (5)$$

represents the $|\bar{2}5\rangle$ charge-transfer configuration. Our notation is such that $(-\odot-)$ represents a neutral site in the ground-state configuration, $(-\oplus-)$ a site with a hole, $(-\ominus-)$ a negatively charged site with an excess electron, and $(-\otimes-)$ a neutral excitonic site.

System-specific information is incorporated by using valence and conduction band Wannier functions (WFs) $|\bar{m}\rangle$ and $|m\rangle$ as the single particle basis. For the single-particle band-structure we use a Hartree–Fock Pariser–Parr–Pople (PPP) approximation that can be parameterized easily for a variety of luminescent conjugated polymer systems and uses this to construct maximally optimized Wannier functions. The single-particle terms, F^o_{mn}, are derived at the ground-state equilibrium configuration, $q_\mu = 0$, from the Fourier components f^o_r and $\bar{f}^o_r$ of the band energies in pseudomomentum space:

$$F^o_{mn} = \delta_{\bar{m}\bar{n}}\langle m|f^o|n\rangle - \delta_{mn}\langle\bar{m}|\bar{f}^o|\bar{n}\rangle = \delta_{\bar{m}\bar{n}} f^o_{m-n} - \delta_{mn}\bar{f}^o_{\bar{m}-\bar{n}}. \quad (6)$$

Here, f_{mn} and $\bar{f}_{mn}$ are the localized energy levels and transfer integrals for conduction electrons and valence-band holes. For alternate conjugated systems, such as PPV, these terms obey charge–conjugation (i.e., e–h symmetry) with $\bar{f}_r = -f_r$. At the ground-state equilibrium geometry, $q_\mu = 0$, these terms can be computed as Fourier components of the one-particle energies in the Brillouin zone.* For example, for the conduction band

$$f^o_{mn} = f^o_{m-n} = \frac{1}{B_z}\int_{B_z} \varepsilon^o_k e^{ik(m-n)} dk, \quad (7)$$

where k is the pseudomomentum for a 1-D lattice with unit period. For the case of cosine-shaped bands, the site energies are given by the band-gap at $k = \pi$ and the nearest-neighbor transfer integral by the bandwidth. The WFs themselves are constructed in a similar way via unitary transformation of the Bloch orbitals:

$$w_i(r) = \frac{1}{B_z}\int_{B_z} e^{ikr}\phi_{k,n,s}(r) dk. \quad (8)$$

Taking inversion symmetry of PPV into account allows us to define real WFs centered either on the vinylene or phenyl portion of each repeating unit. In our implementation, we use WFs centered on the vinylene centers because these tend to be more localized [17].

The two-particle interactions are spin dependent with

*Superscript 0 applies to quantities, taken at ground-state equilibrium, e.g., $q_\mu = 0$.

$$V^{T}_{mn} = -\langle m\bar{n}\|n\bar{m}\rangle \tag{9}$$

$$V^{S}_{mn} = V^{T}_{mn} + 2\langle m\bar{n}\|\bar{m}n\rangle \tag{10}$$

with

$$\langle m\bar{n}\|\bar{i}\bar{j}\rangle = \int d1 \int d2 \phi^{*}_{m}(1)\phi^{*}_{\bar{n}}(2)v(12)\phi_{i}(1)\phi_{\bar{j}}(2).$$

With the exception of geminate WFs, orbital overlap is small such that the two-body interactions are limited to Coulomb and exchange integrals reflecting e–h attraction and spin–exchange coupling nongeminate configurations:

$$J_{|m-n|} = \langle m\bar{n}\|m\bar{n}\rangle = J_{o}(1 - r/r_{o})^{-1} \tag{11}$$

$$K_{|m-n|} = \langle m\bar{n}\|\bar{n}m\rangle = K_{o}\exp(-r/r_{o}) \tag{12}$$

and transition dipole–dipole integrals coupling only geminate singlet electron–hole pairs,

$$D_{|m-n|} = D_{o}(r/r_{o})^{3}. \tag{13}$$

Finally, the electron–phonon coupling term, $H_{\mathrm{el-ph}}$, describes the local variation of the single-particle band gap and is taken to be linear a set of phonon normal-mode coordinates q_{μ} that are localized within a single-unit cell. The linear coupling strength for both the electron and holes, $(\partial f/\partial q_{\mu})_{o} = -(\partial \bar{f}/\partial q_{\mu})_{o}$, is adjusted empirically to reproduce the vibronic progressions observed in the single-photon absorption and emission spectra. Correspondingly, the vibrational term, H_{ph}, models the weakly dispersive optical phonon branches in the frequency ranges of the dominant Franck–Condon active modes observed in the experimental spectra. For the case of PPV considered here, the phonon term consists of two sets of local harmonic oscillators with weak nearest-neighbor coupling, representing two dispersed optical phonon branches, centered at 1600 and 100 cm^{-1}, respectively. These frequencies roughly correspond to C═C bond stretches and ring-torsional motions (librations), which dominate the Franck–Condon activity in PPV and related polymers [20,22]. Huang–Rhys factors (dimensionless el–ph coupling constants) for S_1 of the isolated monomer were subsequently set to 0.8 for the high-frequency mode and 10 for the low-frequency mode. We recently showed that this model is capable of reproducing the vibronic absorption and emission spectra of PPV oligomers from 2–32 repeating units [17].

DIABATIC REPRESENTATION

Having set up the primitive Hamiltonian and parameterized it according to a model physical system, we can obtain the diabatic electronic/vibrational structure by separately diagonalizing H_{el} and H_{ph} yielding a series of vertical excited states with energies ε^{o}_{a} (from $q_{\mu} = 0$) and normal modes with frequencies ω_{ξ}. Written in the diabatic representation

$$\tilde{H} = \sum_{a} \varepsilon^{o}_{a}|\mathbf{a}\rangle\langle\mathbf{a}| + \frac{1}{2}\sum_{\xi}(\omega^{2}_{\xi}Q^{2}_{\xi} + P^{2}_{\xi}) + \sum_{ab\xi} g^{o}_{ab\xi}Q_{\xi}|\mathbf{a}\rangle\langle\mathbf{b}|. \tag{14}$$

The diabatic coupling term $g^{o}_{ab\xi}$ is simply the original electron–phonon coupling tensor transformed into this new representation. The density of states (DOS) for vertical singlet and triplet excitations from the ground state for a PPV model with 32 repeat units (PPV_{32}) is shown in Figure 1, as parameterized from the π-band structure and Wannier functions of the extended polymer. Although the Stokes shift from adiabatic relaxation of the excited states is missing in this calculation, the lowest singlet S_1 and triplet T_1 excitons differ significantly in terms of their binding energies. Here, T_1 is roughly 1 eV lower than the S_1, in general agreement with experimental and theoretical estimates. We can also use the diabatic representation to calculate the relaxed excited states and their respective potential energy curves. This we achieve by variational minimization of the adiabatic energy $\varepsilon_{a} = \langle\mathbf{a}|\tilde{H}|\mathbf{a}\rangle$ of each individual state according to

$$\frac{\partial \varepsilon_{a}}{\partial Q_{\xi}} = g_{aa\xi} + \omega^{2}_{\xi}Q_{\xi} = 0. \tag{15}$$

The relaxed excited states are eigenstates of $\tilde{H}_{\mathrm{el}} + \tilde{H}_{\mathrm{ph}}$ at state-specific conformations, $Q_{\xi,a} \neq 0$, displaced from the ground state at $Q_{\xi} = 0$. Such displacements modify the optical spectra by moving states into and out of regions of strong Franck–Condon coupling to the ground state [23, 24]. Thus, we can test the parameterization of the model by computing the Condon spectral density

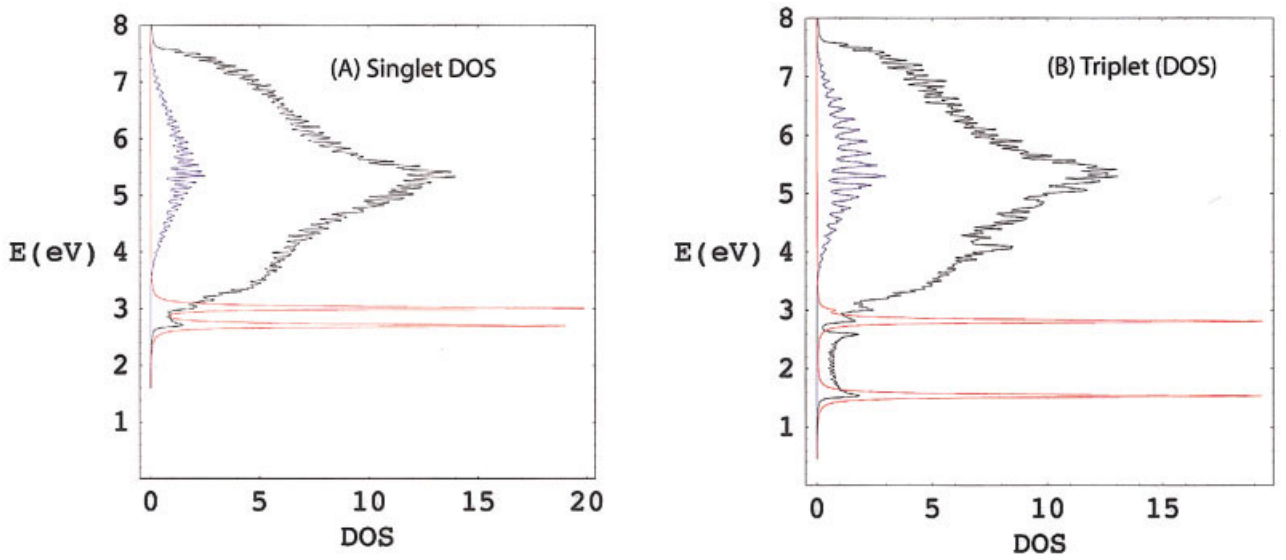

FIGURE 1. Density and population of (A) singlets and (B) triplets. Density of states, black; initial population, blue; relaxed population (symmetrical band structure), red. [Color figure can be viewed in the online issue, which is available at www.interscience.wiley.com.]

for single photon absorption. The cumulative spectral density of PPV_{32} is given in Figure 2 for both the vertical and Condon approximation. Individual electron–vibrational transitions are taken to give Lorentzian lineshapes of half-width 0.01 eV. The oscillator strengths for the $S_o \rightarrow S_a$ vertical transitions were computed by assuming that only geminate and nearest-neighbor e–h pairs are dipole coupled to S_o. Because S_1 is approximately an all-symmetrical combination of such configurations, the bulk of the spectral density is concentrated in this state. Further, the $S_o \rightarrow S_1$ vibronic band is peaked in the $0 \rightarrow 1$ C═C stretching feature, in agreement with the experimental spectra. Vibronic structure from librations is smeared and produces spectral broadening proportional to Huang–Rhys factors times phonon frequencies. The low-frequency coupling also determines the ≈0.15-eV Stokes shift of the $0 \rightarrow 0$ C═C stretch feature from the adiabatic origin of S_1 at 2.34 eV.

RELAXATION DYNAMICS

Separated CT states are not eigenstates of the diabatic Hamiltonian and will evolve in time according to the time-dependent Schrödinger equation. Unfortunately, a complete description of the vibronic dynamics is unfeasible due to the enormous size of the state space. However, we can consider the phonons as a dissipative finite-temperature bath for the electrons and derive reduced equations of motion for the electronic dynamics. For this we turn to the Liouville–von Neumann equation for the evolution of the electronic density matrix

$$i\hbar\dot{\rho} = [\tilde{H}_{\mathrm{el}}, \rho] + \frac{i}{\hbar}\mathcal{R}\rho, \tag{16}$$

where the first term represents the unitary evolution of the uncoupled electronic states in the diabatic representation and the second term the nonunitary, dissipative dynamics due to the coupling to the phonon bath. Because the electronic-state space consists of roughly 100 energy levels, we restrict our attention to the population dynamics and decouple populations from coherences according to the Bloch model:

$$\mathcal{R}_{aabb} = -k_{ab} + \delta_{ab}\sum_c k_{ac} \tag{17}$$

$$\mathcal{R}_{abab} = \frac{1}{2}\sum_c (k_{ac} - k_{bc}), \tag{18}$$

where k_{ab} are the rates of elementary interstate transitions. For internal conversions within the diabatic excited states, we assume that the pho-

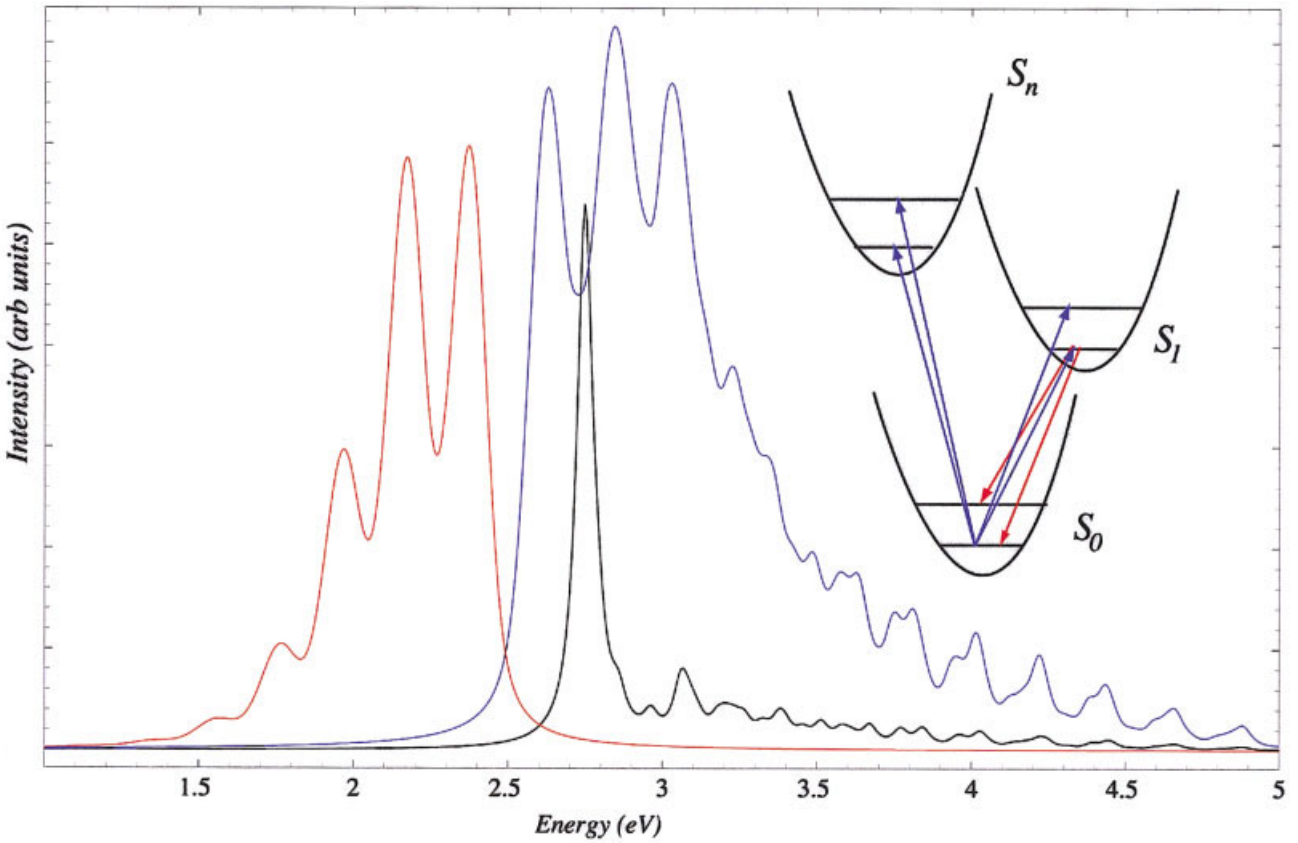

FIGURE 2. Computed Condon spectral densities for $(PPV)_{32}$. Absorption (blue) and red-shifted emission (red) spectra between the adiabatic ground state and the excited states and the black curve is the oscillator strength for vertical excitation from the ground state. Spectral features correspond to excitation of C═C vibronic stretching modes in the excited state (upon absorption) and in the ground state (upon emission) as detailed in the inset. [Color figure can be viewed in the online issue, which is available at www.interscience.wiley.com.]

nons thermalize rapidly on the time scale of the electronic dynamics such that the one-phonon transition rates can be determined within the Markov approximation:

$$k_{ab} = \pi \sum_{\xi} \frac{(g^{o}_{ab\xi})^2}{\hbar\omega_{\xi}} (n_{\xi} + 1)(\Gamma(\omega_{\xi} - \omega_{ab}) - \Gamma(\omega_{\xi} + \omega_{ab})). \tag{19}$$

Here, n_{ξ} is the Bose–Einstein distribution of phonons at $T = 300$ K and Γ is the empirical broadening of 0.01 eV. Note that for an elementary $a \rightarrow b$ population transfer to occur there must be a phonon mode ω_{ξ} at that transition frequency ω_{ab}. Thus, phonon-mediated dynamics is restricted to the excited-state manifold where the energy level spacing is commensurate with the phonon energies. In contrast, single-photon processes occur across the $S_o \rightarrow S_1$ optical gap and the rate of spontaneous emissions is given by

$$k_{a0} = \frac{|\mu_{a0}|^2}{6\epsilon_o\hbar^2}(1 + n(\omega_{a0}))\frac{\hbar\omega^3_{a0}}{2\pi c^3}, \tag{20}$$

where μ_{a0} are the transition dipoles of the excited singlets. These we can compute directly from the Wannier functions or empirically from the photoluminescence decay rates for a given system. Photon-mediated transitions between excited states are highly unlikely due to the ω^3_{ab} density factor of the optical field. In essence, so long as the nonequilibrium vibrational dynamics is not a decisive factor, we can use these equations to trace the relaxation of an electronic photo- or charge-transfer excitation from its creation to its decay including photon outflow measured as luminescence.

TABLE I
Collected data for various chain lengths (symmetrical case).

n	$E_S - E_T$ (eV)	τ_S (ps)	τ_T (ps)	r	ϕ
2	1.552	29.3541	20.4905	0.698	0.19
4	1.309	23.0852	30.4756	1.323	0.31
8	1.199	18.8897	49.8341	2.646	0.47
16	1.174	17.1152	60.9348	3.560	0.54
32	1.146	17.8005	174.771	9.818	0.77

τ_S and τ_T are the formation half-times [$\tau = \ln(2)/k$], $r = k_s/k_t$, and $\phi = r/(r + 3)$ is the electroluminescent efficiency.

Electron–Hole Capture Kinetics

CAPTURE CROSS-SECTION AND CHAIN LENGTH

In modeling of e–h capture, propagation starts from the free e–h pair represented by the charge-transfer (CT) configuration with an electron and a hole on the far ends of the polymer chain; for example,

$$|\psi_0\rangle = (\ominus - \odot - \cdots - \odot - \oplus). \quad (21)$$

We considered chains with $n = 2$, 4, 8, 16, and 32 repeat units corresponding to longer and longer polymer chains. The salient data from each of these calculations is presented in Table I. In Figure 1 we show the diabatic DOS and the spectral distribution of the starting configuration in S and T state spaces for a 32-repeat-unit chain $(PPV)_{32}$. Singlet and triplet populations are also given at an intermediate stage of relaxation at 100 ps. In both cases, the system evolves to a metastable superposition state, where half of the density remains locked in CT states (S_{CT} or T_{CT}) above the lowest excitons (S_{XT} or T_{XT}).* The branching into CT and XT channels is due to e–h symmetry, which separates excited states into even and odd representations under e–h transposition. Thus, XT states, which are even, are not vibronically coupled to CT states, which are odd. As shown in Figure 3(a), S_{XT} and T_{XT} are formed at different rates. Whereas S_{XT}, S_{CT}, and T_{CT} show almost parallel population growths, formation of T_{XT} is far slower.

*By S_{XT} we mean S_1 and the several other thermally populated singlets above it (similarly for T_{XT}, S_{CT}, and T_{CT}).

Assuming that after an initial approach time the formation of the lowest-energy excitons follows first-order kinetics corresponding to the decay of some precursor state, we can fit the population data to an exponential form and obtain the formation rate constants. For the longest chain considered ($(PPV)_{32}$), the formation half-times are $\tau(S_{XT}) = 17.80$ ps and $\tau(T_{XT}) = 174.77$ ps, i.e., $r = 9.8$, corresponding to a 77% EL/PL efficiency, which is systematically higher than observed in both LED [3, 28] and PADMR [4] data but nevertheless consistent with the observed trend. For physical systems in which disorder limits the effective conjugation length, one might expect the effective conjugation length to be more on the order of 8–10 repeat units. For PPV this corresponds to $r \approx 3$, which is more in line with the experimental observations.

The intrinsic distinction between S and T e–h captures is readily understood in terms of different exciton binding energies [8–11] ($\varepsilon_B = \varepsilon_{CT} - \varepsilon_{XT}$). As seen in Figure 1, the singlet excitonic band S_{XT} nearly overlaps with the charge-transfer band S_{CT}, whereas in the case of the triplet exciton T_1 lies at the bottom of a separate band of bound e–h pairs, about 1.5 eV below the CT continuum. Thus, T_{XT} formation requires on average a longer sequence of vibron-mediated transitions, each falling into the phonon frequency range.

BREAKING E–H SYMMETRY

The higher efficiency of S recombination becomes more apparent when e–h symmetry is lifted. We slightly broaden the conduction band and squeeze the valence band so that $f/\bar{f} = -1.1$. The small e–h asymmetry changes negligibly the electronic spectrum but opens a weak vibronic channel for CT $\rightarrow$ XT internal conversions. The resulting population dynamics are shown in Figure 3(b). Here, we see a fast build-up of low-lying XT and CT states in the first 100 to 200 ps, followed by a slow conversion of CT states into excitons. The initial dynamics occurs approximately without e–h parity crossovers and the formation rates of low-lying XT and CT singlets and triplets are about the same as in the symmetrical case. However, the triplet XT to CT branching ratio decreases rapidly to about 1:2 and suppresses the formation of T_{XT}. Moreover, subsequent $T_{CT} \rightarrow T_{XT}$ relaxation is slow due to the large binding energy of triplet excitons and the low density of states between T_{CT} and T_{XT}. Thus, the T_{XT} population reaches only 40% after 800-ps propagation. In contrast, S_{XT} is slightly favored over S_{CT} in

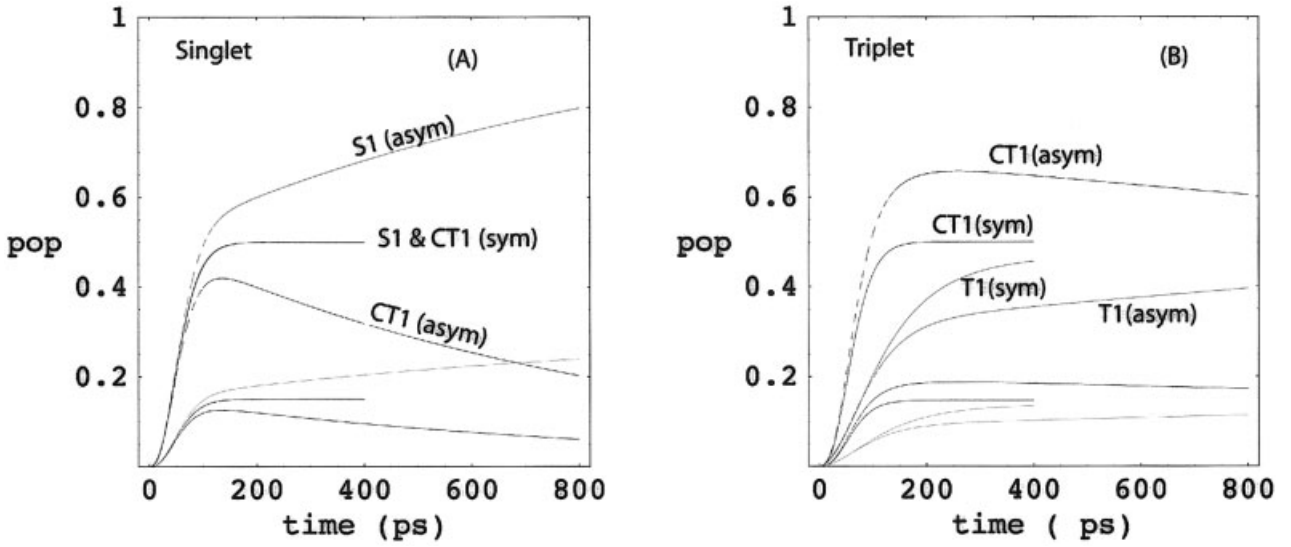

FIGURE 3. e–h capture population dynamics of essential states with and without e–h symmetry for (A) singlet and (B) triplet cases. Solid curves are with e–h symmetry enforced and broken curves are for broken e–h symmetry. In both figures, we show the population dynamics for the lowest two excitonic and charge-transfer states. [Color figure can be viewed in the online issue, which is available at www.interscience.wiley.com.]

the initial capture, and further $S_{CT} \rightarrow S_{XT}$ conversion occurs on a timescale of about 800 ps [18].

Note as well that S_{CT} and T_{CT} are close in energy because of the lack of appreciable exchange between separated electrons and holes. Hence, intersystem $S \rightarrow T$ crossing of long-lived CT states due to spin–orbit coupling (not included in the present model) is highly likely to occur prior to final e–h binding.

ANALYTIC MODEL: UNIVERSAL SCALING RELATION

Consider the relaxation from the lowest unbound (CT) state to the lowest bound excitonic (XT) state due to coupling to the lattice vibrations. Because the exciton binding energy is greater than the energy for a single phonon transition, we need to think about this as a multiphonon process. If we assume that this occurs as a set of discrete hops of energy $\delta E \approx \hbar\omega_{\text{phonon}}$, then the binding energy is $\varepsilon_B = N\delta E$. Further, if we assume that the transition rate is constant between adjacent vibronic levels, k is the same for all steps, then the population of an intermediate vibronic sublevel is given by the kinetic equations

$$\dot{n}_i = k(n_{i+1} - n_i) \tag{22}$$

for $0 < i < N$ and

$$\dot{n}_N = -kn_N(t) \tag{23}$$

$$\dot{n}_0 = +kn_1(t) \tag{24}$$

for the initial and final states. We assume that downward transitions ($i + 1 \rightarrow i$) are favored over upward transitions. For systems at low temperature, this will be the case so long as $k_BT < \delta E$. The kinetic equations are best represented in matrix form:

$$\begin{pmatrix} \dot{n}_N(t) \\ \dot{n}_{N-1}(t) \\ \vdots \\ \dot{n}_1(t) \\ \dot{n}_0(t) \end{pmatrix} = k \begin{pmatrix} -1 & 0 & \cdots & 0 & 0 \\ 1 & -1 & 0 & \cdots & 0 \\ \vdots & \ddots & \ddots & \ddots & \vdots \\ 0 & \cdots & 1 & -1 & 0 \\ 0 & \cdots & 0 & 1 & 0 \end{pmatrix} \begin{pmatrix} n_N(t) \\ n_{N-1}(t) \\ \vdots \\ n_1(t) \\ n_0(t) \end{pmatrix}, \tag{25}$$

i.e.,

$$\dot{P}(t) = k\mathcal{J}P(t). \tag{26}$$

Here, $P(t)$ is a vector of populations with $P(0) = \{1, 0, \ldots, 0\}$ and $k\mathcal{J}$ is the kinetic matrix. This equation can be solved (formally) by exponentiation of the kinetic matrix

$$P(t) = \exp[k\mathcal{J}t] \cdot P(0). \tag{27}$$

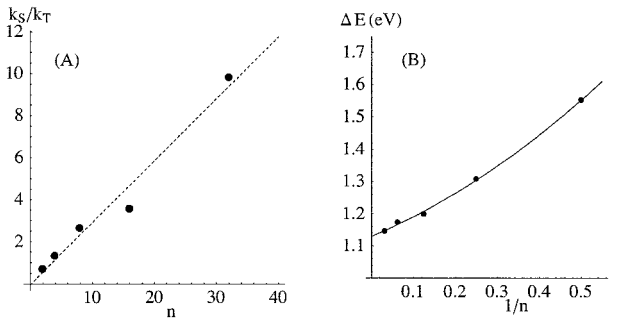

FIGURE 4. (A) Linear relation between polymer chain length, n, and the rate constant ratios for singlet and triplet cases. (B) Singlet–triplet gap vs. $1/n$. The solid curve is fit to a quadratic form.

Next, expand the exponential as a polynomial in $k\mathcal{J}t$. Because the upper $N \times N$ block is in Jordan form, the sum converges after a few terms. For example, for the case where $N = 5$ the matrix representation of $\exp[k\mathcal{J}t] \cdot P(0)$ yields

$$e^{-kt}\begin{pmatrix} 1 \\ kt \\ \frac{k^2t^2}{2} \\ \frac{k^3t^3}{6} \\ \frac{k^4t^4}{24} \\ \left(e^{kt} - 1 - kt - \frac{k^2t^2}{2} - \frac{k^3t^3}{6} - \frac{k^4t^4}{24}\right) \end{pmatrix}. \quad (28)$$

The population of the XT level is the last entry in this array:

$$n_0(t) = 1 - e^{-kt}\left(1 + kt + \frac{k^2t^2}{2} + \frac{k^3t^3}{6} + \frac{k^4t^4}{24}\right).$$

Carrying out this analysis for arbitrary number of energy levels yields

$$n_0(t) = n_{\mathrm{XT}}(t) = 1 - e^{-kt}\sum_{i=0}^{N-1}\frac{(kt)^i}{i!}. \quad (29)$$

This simplifies to

$$n_{\mathrm{XT}}(t) = 1 - \frac{\Gamma(n, kt)}{\Gamma(n)}, \quad (30)$$

where $\Gamma(a, b)$ is the incomplete Euler gamma function:

$$\Gamma(a, z) = \int_z^\infty t^{a-1}e^{-t}dt.$$

Now we ask, what is the time required for exactly one half of the initial population to appear in the lowest state ($i = 0$) starting from the highest ($i = N$)? In the situation derived here, this occurs where $n_{\mathrm{XT}}(t)$ passes though an inflection point. Thus, we need to solve

$$\frac{d^2n_{\mathrm{XT}}(t)}{dt^2} = e^{-kt}(kt)^N\frac{(N - 1 - kt)}{t^2\Gamma(N)} = 0 \quad (31)$$

for the inflection time. This occurs at $t_{1/2} = (N - 1)/k$. Hence, $t_{1/2}$ scales linearly with the number of intermediate states and, consequently, the binding energy because $\varepsilon_B = N\delta E$. Thus,

$$r = \frac{\tau_T}{\tau_S} \propto \frac{\varepsilon_B^T}{\varepsilon_B^S}, \quad (32)$$

which is consistent with our simulations discussed above.

Next, we take the singlet–triplet energy gaps (Fig. 4) into consideration. To a lowest-order approximation the singlet–triplet energy difference is approximately equal to twice the e–h correlation energy $\Delta E_{\mathrm{ST}} = 2K$. Using the data in Table I, we can fit ΔE_{ST} to a simple functional form

$$\Delta E_{\mathrm{ST}} = K_\infty + K^{(1)}/n + K^{(2)}/2n^2, \quad (33)$$

where $K_\infty = 1.13$ eV, $K^{(1)} = 0.55$ eV, and $K^{(2)} = 0.30$ eV, where n is the chain length. Thus,

$$r \propto \frac{\varepsilon_B^T}{\varepsilon_B^S} = \frac{\varepsilon_B^S + \Delta E}{\varepsilon_B^S} \tag{34}$$

$$\propto \frac{\varepsilon_B^S + K_\infty + K^{(1)}/n + K^{(2)}/n^2}{\varepsilon_B^S}. \tag{35}$$

Finally, using $\varepsilon_B^S \propto 1/n$, we obtain

$$r \propto 1 + K^{(1)} + nK_\infty + \mathbb{O}(K^{(2)}/n). \tag{36}$$

Because K_∞ is twice the correlation energy of an e–h pair in an infinitely long chain, as we can assume that for organic polymers, its value is more or less system independent. This universality is consistent with the experimental observations reported in Ref. [5]. Thus, we argue that the recombination process proceeds via a cascade through a series of intermediate states coupling the lowest charge-transfer states to the lowest excitonic state.

Conclusion

In summary, we simulated phonon-mediated intrachain e–h recombination in LCPs. The approach allows us to examine EL quantum yield in LCPs further case by case by combining a first-principle description with available spectroscopic data. While we focus here on PPV and adjust el–ph coupling to its absorption spectrum, results can be generalized to most nondegenerate polymers. Apart from spin-degeneracy statistics, efficiency of singlet e–h capture outweighs the triplet one as a natural outcome of the higher binding energy of triplet excitons. For both S and T processes, the relaxation mechanism involves two steps as a result of approximate e–h symmetry. In the initial e–h capture, both low-lying excitons and same-spin CT intermediates are formed. The XT to CT branching ratio may vary but is inevitably more favorable for singlet excitons than for triplet ones simply due to energetics. Relaxation to the higher-lying singlet exciton requires fewer elementary relaxation steps than the lower-lying triplet exciton. Subsequent conversion of CT states into excitons is forbidden by e–h symmetry and occurs on a much slower timescale once this symmetry is broken. The weak e–h asymmetry of real conjugated systems favors again the singlet CT $\rightarrow$ XT relaxation by a factor commensurate with the ratio of T to S exciton binding energies.

What is desired is experimental detection of the transient kinetics we predict in our model. Ideally, the experiment would monitor the fluorescence signal following e–h injection onto a polymer chain. This is an extremely difficult experiment because electroinjection typically entails multiple polymer chains with disordered morphology. This is a significant lacuna in our current model and we have begun work on incorporating multiple polymer chains into our theory to model interchain e–h transfer and recombination dynamics.

What is also curious is our predictions and the observation that the EL efficiency is dependent upon the rate of formation of emissive states. This implies that the formation rate constant should be the limiting factor in the recombination process following electroinjection and not the e–h diffusion time. Surprisingly, the diffusion times for charge carriers are significantly longer than the recombination rates reported herein and for that matter predicted by other groups. Moreover, because carrier diffusion is more or less independent of spin state (due to the fact the carriers are noninteracting), one expects that the EL efficiency to not depend upon the recombination process and should reflect the 1:3 ratio of singlets to triplets in the system. We hope that further experimental and theoretical work will shed some additional light onto the electroluminescence mechanism in organic polymers.

ACKNOWLEDGMENTS

This work was funded by the National Science Foundation and the Robert A. Welch Foundation. E.R.B. thanks the organizers of the 2003 Sanabel Symposium and John Wiley & Sons, Inc. for the Wiley *International Journal of Quantum Chemistry* Young Investigator Award.

References

1. Burroughes, J. H. et al. Nature 1990, 347, 539.
2. Friend, R. H. et al. Nature 1999, 397, 121.
3. Cao, Y. et al. Nature 1999, 397, 414.
4. Wohlgenannt, M. et al. Nature 2001, 409, 494.
5. Wohlgenannt, M.; Jiang, X. M.; Vardeny, Z. V.; Janssen, R. A. J. Phys Rev Lett 2002, 88, 197401.
6. Shuai, Z. et al. Phys Rev Lett 2000, 84, 131.
7. Ye, A.; Shuai, Z.; Bredas, J. L. Phys Rev B 2002, 65, 5208.
8. Kobrak, M.; Bittner, E. R. Phys Rev B 2000, 62, 11473.
9. Bittner, E. R.; Kobrak, M. N. Synth Met 2001 (in press).

10. Bredas, J. L.; Cornil, J.; Heeger, A. J. Adv Mater 1996, 8, 447.
11. Bredas, J. L. et al. Acc Chem Res 1999, 32, 267.
12. Burin, A. L.; Ratner, M. A. J Chem Phys 1998, 109, 6092.
13. Tandon, K.; Ramasesha, S.; Mazumdar, S. Phys Rev B 2003, 67, 45109.
14. Wohlgenannt, M.; Vardeny, Z. V. J Phys Condens Matter 2003, 15(3), R83.
15. Mukhopadhyay, D.; Hayden, G. W.; Soos, Z. G. Phys Rev B 1995, 51, 9476.
16. Chandross, M.; Shimoi, Y.; Mazumdar, S. Phys Rev B 1999, 59, 4822.
17. Karabunarliev, S.; Bittner, E. R. J Chem Phys 2003, 118, 4291.
18. Karabunarliev, S.; Bittner, E. R. J Chem Phys (in press).
19. Karabunarliev, S.; Bittner, E. R. Phys Rev Lett 2003, 90, 57402.
20. Hagler, T. W.; Packbaz, K.; Heeger, A. J. Phys Rev B 1994, 49, 10968.
21. Pichler, K. et al. J Phys Condens Matter 1993, 5, 7155.
22. Cornil, J. et al. Chem Phys Lett 1997, 278, 139.
23. Karabunarliev, S.; Bittner, E. R.; Baumgarten, M.; Müllen, K. J Chem Phys 2000, 113, 11372.
24. Karabunarliev, S.; Bittner, E. R.; Baumgarten, M. J Chem Phys 2001, 114, 5863.